CRITICAL REVIEW

Check for updates

Microneedle-integrated wearable devices for healthcare monitoring

Tianli Hu, [iD] Eira Beryle Ko, Yu Song and Chenjie Xu [iD] *

Wearable technologies have emerged as powerful tools for non-invasive healthcare monitoring, enabling continuous detection of biomarkers to support personalized medicine and disease management. However, most biological biomarkers stay inside tissue and cannot be accessed on the skin surface through simple contact. Microneedle (MN) technology provides a solution for the wearable technologies to sample biofluid, detect biomarkers, and monitor electrophysiological signals. This article provides a comprehensive overview of the latest development in this field, highlighting MN design principles, functional integration with microfluidics, microelectronics, and artificial intelligence as well as the practical applications. We conclude by discussing the challenges in technical development, clinical validation, industrialization and regulatory compliance, as well as future prospects for MN-integrated wearable devices.

1. Introduction

Continuous healthcare monitoring facilitates personalized management of chronic conditions and improves overall wellbeing.[1] Conventional practices require patients to be physically present at the clinics for sampling and diagnosis, which is inconvenient, time-consuming and offers only intermittent assessment of the patient's health status. The emergence of wearable biomedical devices has opened a new area of personalized health monitoring by accurately measuring physical states and biochemical signals without the need of presence at clinics.[2,3]

Signals monitored by wearable devices can be classified into physical signals and chemical signals. Physical signals refer to pressures and motions, such as touch and heart pulse. They can be detected through electromechanical sensors attached on the skin.[4–7] Chemical signals refer to ions/molecules that transmit information between cells (e.g. glucose, sodium ions, uric acid, antibodies or hormones).[8] They exist in biofluids including blood, sweat, saliva, and tears. The sensors must access the fluid before converting them to useful signals for detection and quantification.[9–13] Certain biofluids like sweat, saliva, and tears can be accessed noninvasively, but their use is limited by challenges such as low biomarker concentrations, environmental contamination, and high variability. Originating from blood plasma that diffuses through capillaries,[14] skin interstitial fluid (ISF) appears as a reliable biofluid with high biomarker

concentration, minimal environmental contamination, and low variability. Many studies have shown that ISF contains biomarkers that are similar in both concentration and composition to that of blood samples, making it a prime candidate for wearable biofluid sensors.[15–17] The only problem is that skin ISF cannot be accessed non-invasively.[18]

Fortunately, the development of microneedle (MN) technology provides a solution. MN devices contain one or an array of needles with lengths from 25 to 2000 μm. MNs have been categorized into solid MNs, coated MNs, hollow MNs, porous MNs and swellable MNs,[19] with morphological variants such as bevelled-tip, cylindrical, pyramidal, and conical profiles[20] (Fig. 1). The MN tips can pierce the stratum corneum and reach the dermis where the ISF stays,[21] which permits a minimally invasive and reliable access to skin ISF. We can either extract ISF using MNs for subsequent analysis or detect the biomarkers in situ by converting them to readable signals through biosensors integrated on MN tips or the backing layer. These MN devices can be further combined with microfluidics, wearable electronics, and artificial intelligence (AI), enabling sampling, quantification, sensing, and data processing in one wearable system. Therefore, we can provide a real-time and minimally invasive approach for disease prevention, early diagnosis, and therapy optimization.

The great potentials of MN technology have driven numerous researchers and other professionals to dedicate their time and resources into MN development. Since 2012, there have been 700 articles published by searching on PubMed with the keywords "microneedle" and "monitoring". The number of publications per year increases with an average annual growth rate of around 58% from 2021 to 2024

Department of Biomedical Engineering, College of Biomedicine, City University of Hong Kong, Kowloon, Hong Kong SAR, China. E-mail: chenjie.xu@cityu.edu.hk
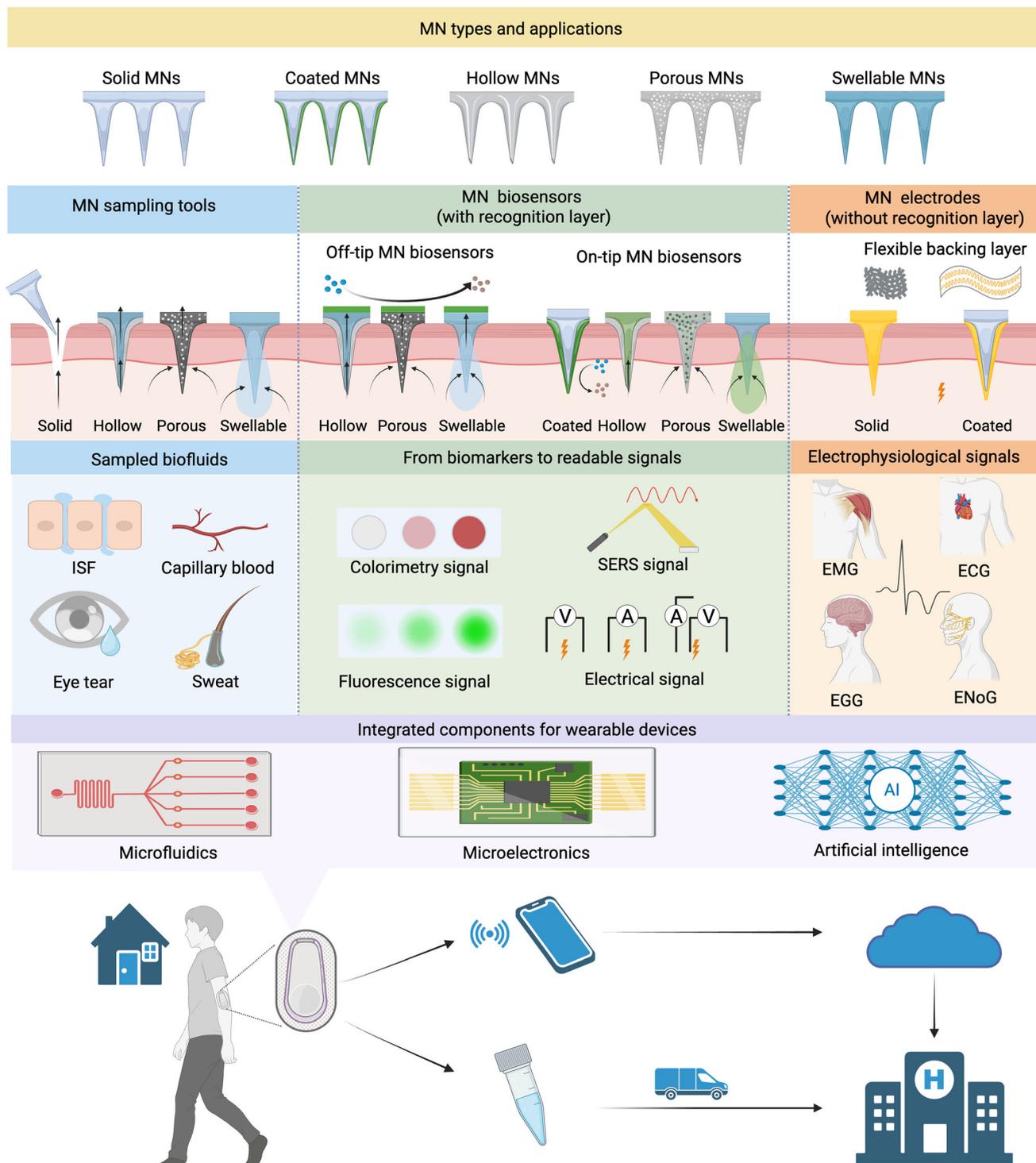
Fig. 1 Integrated wearable MN devices for healthcare monitoring. Abbreviations: MN, microneedle; ISF, interstitial fluid; ECG, electrocardiogram; EMG, electromyography; EEG, electroencephalography; ENoG, electroneurography. Created with **https://BioRender.com**.

(Fig. 2). There are also more than 9 companies in the field of MN sensing (Table 1). In ClinicalTrials.gov, there are 9 registered clinical trials related to MN sensing and sampling technologies (Table 2).

This article overviews the latest development of MN-based wearable devices across three major application domains, including biofluid sampling, biomarker monitoring, and electrophysiological signal acquisition. For each category, we discuss the representative MN designs, integration strategies, and commercialized products, followed by a critical analysis of the key challenges and perspectives for future clinical translation. We realize there
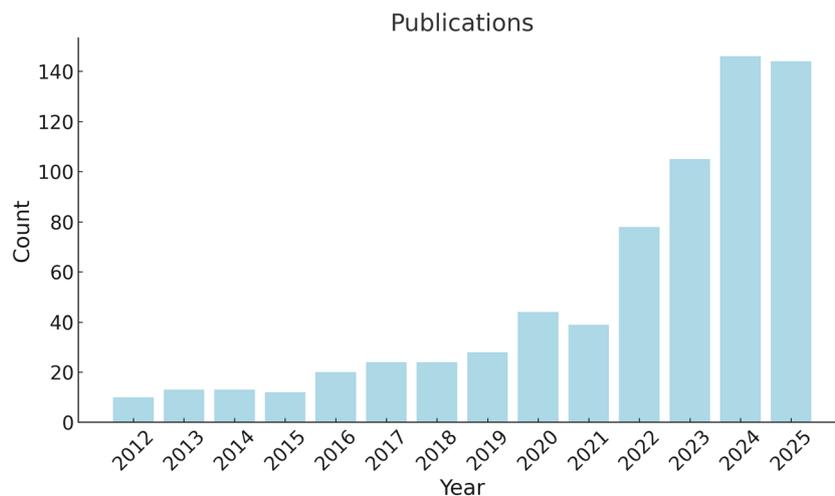
Publications

Fig. 2 Number of publications in PubMed from 2012 to 2025 retrieved using the keywords "microneedle" and "monitoring".

Table 1 Representative companies in the field of MN sensing

Company	Region	MN type	Technology focus	Target analytes
Biolinq	USA	Coated MNs	Intradermal electrochemical MN array for CGM and metabolic biomarkers	Glucose
Dexcom	USA	Retractable hollow MNs	CGM systems employing introducer MN and subcutaneous filament-based electrochemical sensors	Glucose
Abbott	USA	Retractable hollow MNs	CGM platform using introducer MN and filament-based electrochemical sensors	Glucose
CARI Health	USA	Not disclosed	Combining MNs for sensing with remote monitoring, potentially delivering medication on-demand	Methadone, buprenorphine and opioid
SIBIONICS	China	Retractable hollow MNs	CGM system using MN and filament-based electrochemical sensors	Glucose
PKvitality	France	Coated MNs	Smartwatch with disposable MN patch coated with glucose sensing layer	Glucose
WearOptimo	Australia	Solid MNs	MN electrode patch for hydration assessment	Electrolytes
Nutromics	Australia	Coated MNs	DNA-based electrochemical aptamer MN biosensors for multi-analyte detection	Multiple proteins, drugs, metabolites and hormones
Sava	UK	Coated MNs	MN biosensor platform for multi-biomarker monitoring	Glucose
Zimmer & Peacock	UK/EU	Solid/coated MNs	MN arrays and wearable MN sensor prototypes for translational research	Glucose, lactate, ketones, pH, *etc.*

are similar articles published recently. For example, Kim *et al.* presented a comprehensive overview of MN-based sensing for dermal ISF analysis, encompassing skin physiology, MN design, sensing mechanisms, monitoring electronics, and practical applications.[22] Li *et al.* also reviewed MN sensing technology for ISF analysis, covering the fundamental aspects of MNs, including materials, fabrication methods, and structural designs as well as the range of detectable biomarkers.[23] Vora *et al.* highlighted the diverse types of MNs for biosensing, their integration with biosensors, and the clinical applications of wearable MN sensing devices aimed at advancing point-of-care testing.[24] Similarly, Hu *et al.* introduced different classes of MN sensors based on material types, such as metals, inorganics, polymers, and hydrogels, and underscored the importance of commercialization and clinical trials in translating MN technologies into practice.[25] Distinct from these articles, this review presents MN design strategies tailored to specific applications, providing a more focused

perspective rather than a generalized overview of all MN sensor designs. In addition, it highlights the critical role of microfluidics in MN-based wearable devices, such as efficient fluid sample handling and transportation, emphasizing that these systems represent more than a simple combination of MNs and microelectronics. To bridge research and application, we also present commercially available products in each category, thereby providing a market-oriented view that underscores the translational potential of MN technologies.

2. MN-integrated devices for biofluid sampling

MNs can act as a sampling tool to construct a bridge between the biofluids and the reservoir, allowing biofluids like skin ISF and blood to be extracted with the assistance of negative pressure, capillary force, swelling force, or electroosmosis.

Table 2 Registered clinical trials related with MN sensing and sampling from 2016 to 2025

| Year	Clinical trial	Study title	Sponsor	Application(s)	Status	MN device
MN sensing						
2016	NCT02682056	Glucose measurement using microneedle patches (GUMP)	Emory University	ISF glucose monitoring	Completed	MN patch for ISF glucose
2019	NCT03847610	Minimally invasive sensing of beta-lactam antibiotics	Imperial College London	Antibiotic therapeutic drug monitoring	Completed	MN biosensor (electrochemical)
2019	NCT04053140	Closed-loop control of penicillin delivery (CLCPD)	Imperial College London	Closed-loop β-lactam monitoring and control	Recruiting	MN biosensor integrated with control algorithm
2022	NCT05546229	Assessment of methadone and buprenorphine in interstitial fluid	CARI Health, Inc.	Opioid drug level monitoring	Recruiting	MN ISF sensing (electrochemical)
2023	NCT05998876	Assessing dose taken in opioid use disorder with an electrochemical sensor	CARI Health, Inc.	Opioid dose adherence monitoring	Recruiting	MN electrode array
2025	NCT06977633	Feasibility study of a hydrogel microneedle patch for continuous glucose-ketone monitoring	University of Waterloo	Metabolic monitoring (glucose, ketone)	Not yet recruiting	Hydrogel MN patch sensor
MN sampling						
2019	NCT03795402	Microneedle sampling in psoriasis and healthy skin	Janssen Research & Development, LLC	Biomarker/transcriptomics sampling from skin	Completed	MN patch for skin sampling
2025	NCT06934980	Microneedle-based collection of dermal interstitial skin fluid in healthy and AD participants	Incyte Corporation	ISF sampling and biomarker collection	Recruiting	MN patch for ISF collection
2025	NCT06994988	ARPA-H smart band-aid to measure chronic pain in women	Northwestern University	ISF sampling from the skin	Recruiting	A-band wearable MN patch

2.1 Design strategies of MNs

Solid MNs, hollow MNs, porous MNs, and swellable MNs have been studied for biofluid sampling. There are three strategies to use MNs for sampling biofluids from both tissue layers (e.g. ISF and blood) and body surfaces (e.g. sweat and tears).[26–29] The first is to collect biofluids through microchannels created in the skin by solid MNs. These MNs are typically fabricated from materials with high mechanical strength, such as stainless steel[28,30,31] and hard resin.[32] For example, Samant et al. developed a stainless-steel MN array with 5 MNs and a length of 250 μm. After creating micropores in the skin layer, a vacuum pump and gauze were employed to sample microliter volumes of ISF.[29] The solid stainless-steel MNs have also been affixed with absorbent strips that utilized capillary force to collect and store ISF.[28,30,31] Similarly, this methodology can be applied to extract capillary blood. Zoratto et al. developed a cost-effective MN device integrating a hidden circular array of 20–30 stainless-steel MN tips (2 mm length, 13.4° tip angle) within a silicone suction cup and a heart-shaped storage compartment containing K_2-EDTA (Fig. 3A).[33] The device collected roughly 195 μL of blood from piglets within 10 min by generating a negative pressure (~−68 to −73.8 kPa) through silicone's elastic recovery post-compression.

The second strategy utilizes the swelling properties of solid MNs made from hydrogel-forming polymers such as methyl hyaluronate (MeHA),[34–38] gelatin methacryloyl (GelMA),[39,40] and PVA.[41–43] For instance, photo-crosslinked MeHA hydrogel MNs with ~100 MN tips successfully

extracted ~1 mg of ISF from mouse skin within 1 min.[37] The incorporation of maltose as the osmolyte in MeHA MNs further improved their swelling capacity 1.5-fold and ISF extraction volume rose to ~2 μL (mouse skin) in 1 min (Fig. 3B, i and ii).[36]

Finally, we can make use of the MNs' microstructure to extract biofluids. The voids and channels within the hollow or porous MN tips act as conduits, enabling the passive flow of liquid through capillary force.[44] Hollow MNs are currently most popular due to the large lumen.[45–47] For example, an array of 5 syringe needles (32 G, 1500 μm in length), with each needle combined with a glass capillary, achieved an extraction volume of up to 16 μL of ISF from human skin over a 1–2 h period, in contrast to 1.51 μL of ISF collected using a single needle.[45] Silva et al. developed a 3D-printed device with 18 polymer hollow MNs via two-photon polymerization. Each MN is 1 mm in length with an inner diameter of 50 μm and 30 μm side openings. The 3D-printed MNs extracted approximately 1 μL of ISF through hollow channels to microfluidic chambers under 30 kPa pressure and performed consistently in more than 10 insertions (Fig. 3C).[46] Porous MNs can achieve the same goal through the interconnected pores inside the needles.[48–50] For instance, Takeuchi et al. fabricated a porous PDMS MN array by a combination of mold casting and salt leaching techniques, creating pores with diameters ranging from 30 to 60 μm. The MN array, consisting of 169 pyramidal tips each 1200 μm in length, achieved continuous extraction at 0.08 μL min⁻¹ (demonstrated with PBS as an
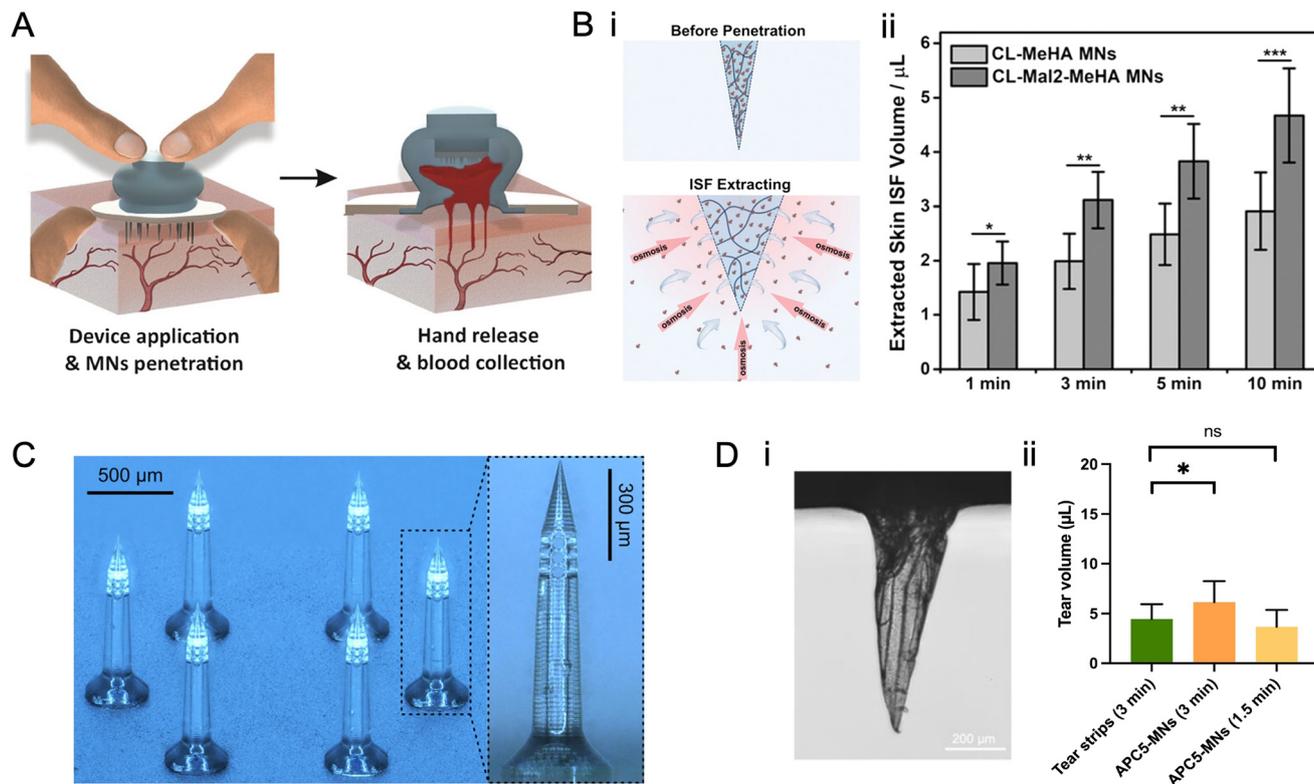
Fig. 3 Representative examples for different types of MNs in biofluid sampling: (A) solid stainless-steel MN array creating micropores in the skin for capillary blood sampling. Reproduced from ref. 33 under the CC-BY 4.0 license. (B) (i) Osmolyte-containing swellable MN array for ISF extraction through the swelling of the hydrogel-forming polymer; (ii) comparison of extracted skin ISF between MeHA MNs and osmosis incorporated MeHA MNs at a range of time points. Reproduced with permission from ref. 36. Copyright 2020, Wiley. (C) Hollow MN array for ISF extraction *via* capillary force. Reproduced from ref. 46. Copyright 2025, Elsevier. (D) (i) Anisotropic porous MNs for tear sampling through the capillary force driven by the aligned channels; (ii) the volume of extracted tears by using anisotropic porous MNs and tear strips from rats with dry-eye disease. Reproduced with permission from ref. 26. Copyright 2025, Elsevier.

ISF substitute) when integrated with microfluidic channels.[49] The aligned porous channels can improve the bioliquid extraction performance. Inspired by the wood xylem structure, we developed MNs with an anisotropic porous architecture that could be used to collect over 5 μL of tears from rat eyes within 3 min (Fig. 3D i and ii).[26] Additionally, grooved MNs have been reported for ISF extraction, with the grooves on the needle surface serving as the primary liquid extraction pathway.[51,52]

2.2 The integration of MNs with microfluidics

The conventional role of sampling MNs is to extract biofluid such as blood, skin ISF, and tears. However, there are several limitations if MNs are used alone for biofluid extraction. Solid MNs act primarily as penetration tools and therefore typically require an additional component to collect and store the extracted fluid. Although swellable, porous, and hollow MNs can retain ISF within their tips and thereby function as self-contained sampling devices; their tip geometry inherently limits the volume of liquid that can be extracted. Consequently, the integration of a biofluid collection component is often necessary to enhance sampling efficiency and capacity, quantify the bioliquid, and ensure sufficient volume for downstream analysis.

Microfluidic technology enables the manipulation of liquids at the microscale, providing precise control over fluid flow, distribution, mixing, and storage. Two main types of microfluidic platforms, paper-based and chip-based ones, have been integrated with MN devices. When paper-based microfluidics is integrated with MNs, biofluids are drawn into the paper strip by capillary forces generated from its fiber structure, thereby enhancing sampling efficiency. The absorbed liquid can be stored within predefined regions of the strip, enabling quantification of the extracted volume. Captured biomarkers can subsequently be recovered using buffer solutions for downstream laboratory analyses.[53,54] For example, Ribet *et al.* developed a device combining a single stainless-steel hollow MN (1 mm length) with a microfluidic chip (Fig. 4A). The MN penetrated into the skin to access ISF, which was guided by microchannels to the defined piece of analytical-grade paper in the chip, enabling the collection of approximately 1.1 μL ISF in ~5 min. The integrated paper reservoir, together with a color indicator, provided built-in volume metering, ensuring a reliable volume metering
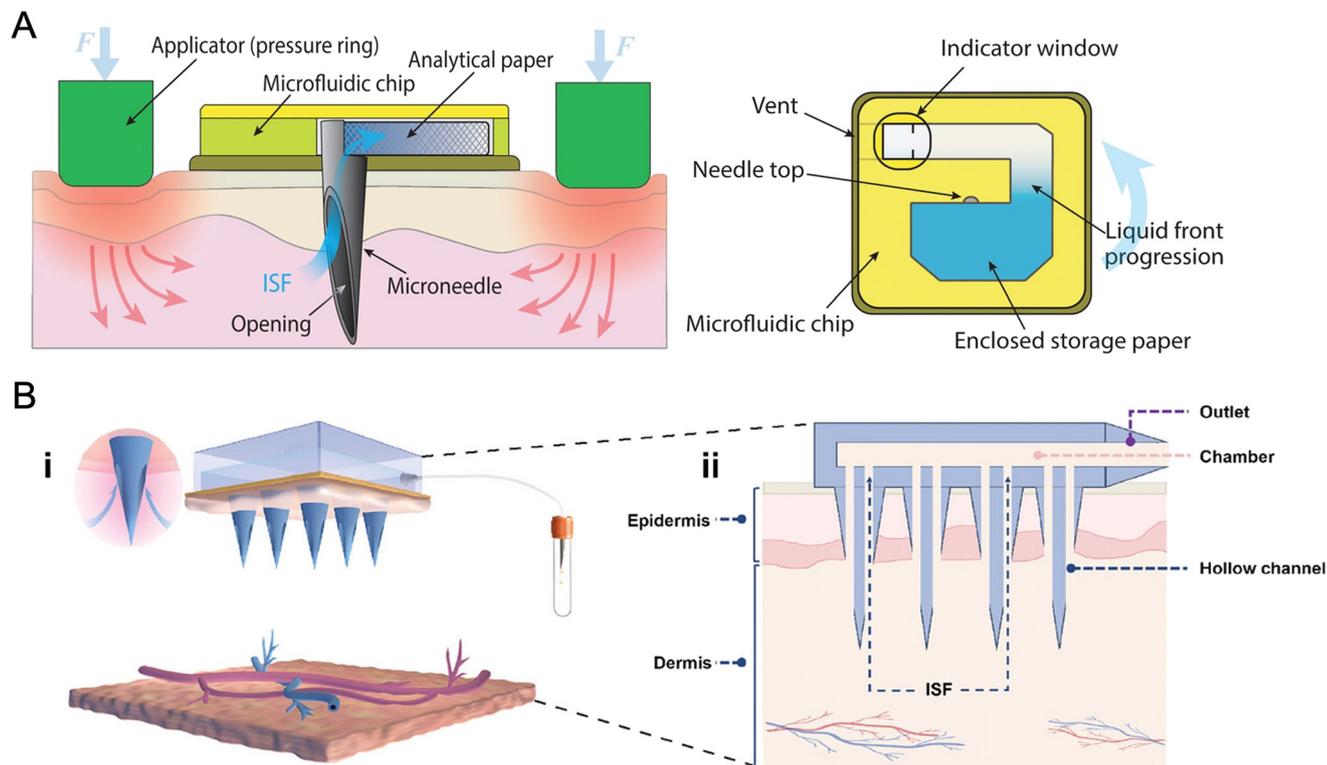
Fig. 4 Integrated wearable MN devices for biofluid sampling. (A) Stainless-steel MN array with silicone suction cup for capillary blood collection. Reproduced with permission from ref. 54. Copyright 2023, Wiley. (B) (i) 3D-printed hollow MN array patch integrated with microfluids for ISF sampling driven by a connected vacuum tube (~18 μL in 5 min); (ii) the cross-section structure of the integrated hollow MN device. Reproduced from ref. 56 under the CC-BY 4.0 license.

(±3.5% variability) for accurate quantification. They further analyzed analytes including caffeine, SARS-CoV-2 antibodies, and hundreds of soluble proteins by liquid chromatography-tandem mass spectrometry (LC-MS/MS) and enzyme-linked immunosorbent assay (ELISA) after recovering the analytes into buffer.[54]

When MNs are integrated with chip-based microfluidics, a vacuum force is typically applied to the microfluidic chip to drive biofluid to flow through the microchannels into a reservoir. This configuration enables precise quantification of the extracted fluid through well-designed microchannels and reservoirs, while the continuous pressure facilitates the sampling of larger volumes.[46,55–57] For instance, Xie et al. developed a 3D-printed hollow MN array integrated with a vacuum tube, merging MN-based sampling with microfluidic chip-based transport (Fig. 4B, i and ii). This setup enhanced biofluid sampling capacity, enabling the extraction of ~18 μL ISF from rabbit ears within 5 min.[56] This integrated design of MNs and chip-based microfluidics has also been applied to sample blood in a painless manner. Blicharz et al. designed a touch-activated phlebotomy (TAP) device that combined a 30-needle stainless-steel MN array (1000 μm length, 350 μm width, 50 μm thickness) with a microfluidic system. It has a snap-dome insertion mechanism, stored vacuum, and microchannels with staggered herringbone mixers to blend blood with lithium heparin. The device

collected 100 μL capillary blood painlessly in ~3 min for diagnostics like HbA1c testing.[58]

2.3 Commercially available MN-based devices for blood sampling

There are several devices that have been commercialized for capillary blood sampling,[59] belonging to class II medical devices under the FDA regulation. One example is the TAP from YourBio Health Inc. (formerly Seventh Sense Biosystems). Powered by HALO™ technology, the device uses a solid MN array (1 mm in length) to penetrate skin. It is significantly less invasive than traditional lancets (2 mm skin penetration depth) or venipuncture (3–10 mm skin penetration depth), avoiding nerve-rich tissue and minimizing pain. The evolution of the TAP device began with the TAP20, which is a one-step, nearly painless device for collecting 20 μL of blood for point-of-care testing released in 2013. It was followed by TAP100, the first-generation model with a 100 μL capacity, which received FDA 510(k) clearance and CE marking. To overcome limitations such as manual pipetting and manufacturing challenges, the second-generation TAP II device introduced detachable tubes for 200–300+ μL blood collection and streamlined processing. The latest model, TAP Micro Select, features modular compatibility with standard collection

tubes and enables home-based capillary whole blood collection of up to 900 μL, with CE marking and FDA 510(k) clearance (Fig. 5A).

Similarly, Tasso Inc. developed a capillary blood collection product, Tasso Mini (Fig. 5B). With a 1.8 mm lancet length and 1.6 mm penetration depth, it is smaller than their other product, Tasso+, which is 3.8 mm in length and 1.8 mm in depth. Its fully integrated lancet and vacuum design enables simple, nearly painless capillary blood collection. Upon activation, the device punctures the skin and gently draws blood into a connected tube. Tasso Mini is compatible with standard 13 mm × 75 mm microtainer tubes and Tasso's own dried blood spot cartridges, offering flexibility for both liquid and dried sample workflows.

Other similar products include Nanodrop and OneDraw from Drawbridge Health Inc. Nanodrop incorporates two stainless-steel needles that penetrate the skin to a depth of 1.9–2.0 mm. Its design includes a plastic housing with a hydrogel adhesive rim, a bow-shaped cavity for vacuum-assisted sampling, activation buttons for vacuum and blade deployment, a yellow lock, and auto-retracting blades after use. The OneDraw blood collection device integrates lancets and a vacuum system to draw blood onto matrix strips within a cartridge. The cartridge, which can maintain its integrity for up to 21 days at room temperature, is then placed into a transport sleeve for secure mailing to a laboratory. Compared to Nanodrop, it is a more streamlined system for sample collection, transport, and analysis.

3. MN-integrated wearable devices for biomarker monitoring

The previous section has listed the criteria and showcased a few examples using MN devices for biofluid sampling. However, to quantitatively analyze the biomarkers in the extracted biofluid, sensing components must be integrated.
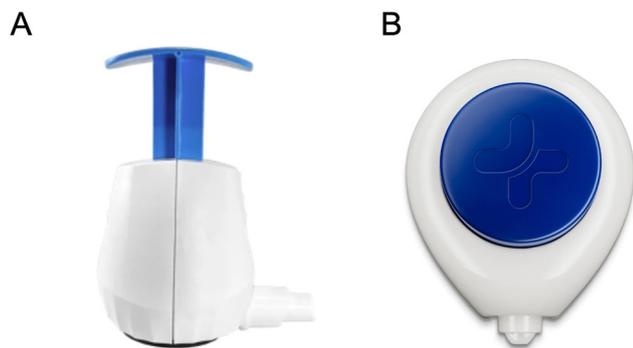
Fig. 5 Representative commercially available MN devices for capillary blood sampling: (A) TAP Micro Select (YourBio Health). Reproduced with permission from YourBio Health Inc. Copyright 2024; https://yourbiohealth.com/. (B) Tasso Mini (Tasso). Reproduced with permission from Tasso Inc. Copyright 2025; https://www.tassoinc.com/.

3.1 Design strategy for MN-based biosensors

MN-based biosensors have been designed as off-tip and on-tip biosensors. In MN devices with off-tip recognition, MNs act as the sampling component while the backing layer of the device contains the sensing element like optical or electrochemical sensors. Hollow MNs, porous MNs, and hydrogel MNs have been used for off-tip MN biosensor development. The extracted biofluid flows from the MN tip to biosensors on the backing layer. The devices with the on-tip sensors carry the recognition assay on the MN tips. Biomarkers are analyzed on the surface of coated MN tips,[60] within the internal physical spaces (lumens or micropores) of hollow and porous MN tips,[61–63] or within the polymer network of hydrogel MN tips.[64–66] Notably, electrochemical on-tip biosensors require materials with excellent conductivity for electrical signal transmission. Conductive materials with high stability and inertness like gold and carbon materials are popular choices in the fabrication, coating, or filling of these MN-based devices.[60,67,68]

The common sensing strategies of both off-tip or on-tip MN-based biosensors convert ISF biological signals into detectable optical or electrical signals. Optical sensing strategies include fluorescence, colorimetry, and surface-enhanced Raman spectroscopy (SERS) assays on- or off-MN tips, recognizing analytes by surface-immobilized fluorophore-conjugated recognition elements,[66,69,70] target-induced chromogenic reagent color changes,[51,71–73] and Raman signals from noble metal nanostructures,[74,75] respectively. On the other hand, electrical biosensors rely on electrochemical signal transduction through amperometric, potentiometric, and voltammetric mechanisms.[22] Amperometric MN sensors measure current from enzymatic redox reactions of ISF metabolites (e.g., glucose,[76] lactate,[77] ketone,[78] etc.). Potentiometric MN sensors use ion-selective membranes to detect ions (e.g., Na^+, K^+, Ca^{2+}) via potential differences.[79,80] Voltammetric MN sensors monitor current responses to varying potentials, with analyte binding altering electron transfer kinetics of immobilized aptamers/antibodies.[81–85] Notably, aptamer-functionalized MN biosensors achieve an ultra-sensitive detection limit of drugs (tobramycin: 1.41 pM; vancomycin: 0.187 nM)[86,87] and metabolites (phenylalanine: fM-level; cortisol: 0.22 nM).[88,89]

3.2 MN wearable devices with off-tip sensors: from independent to integrated use

Off-tip sensors can function independently as wearable devices, enabling biomarker analysis in the biofluids with the biosensing component located at the backing of MNs, such as colorimetric test paper[52,72,90,91] and lateral flow test strips.[92–94] For example, a wax-patterned test paper was combined with swellable MeHA/HA MNs as colorimetric MN sensors. Four specific enzymes and dyes have been incorporated into the test paper to detect glucose, lactate, cholesterol, and pH in the ISF extracted by MNs, enabling visual inspection via color changes.[90] Nevertheless, such detection approaches are limited

to qualitative "yes or no" outputs, as the volume of the analyzed liquid cannot be quantified. Inadequate contact between the sample and the sensing interface may result in unreliable responses, and the precise concentration of target biomarkers cannot be determined.

Integrating off-tip biosensors with microfluidic chips can improve biosensing performance by providing accurate fluidic control, improving analyte–sensor interactions as well as enabling reliable and quantitative assessment of biomarkers. Here, MNs function as the sampling interface, while the microfluidic chip takes roles in fluid guidance, quantification, and storage. The off-tip biosensing components are present in the chamber for converting the biomarker concentrations into readable signals.[95,96] For instance, Chen et al. developed a MN wearable device combining a 6 × 6 hollow MN array with microfluidics and a colorimetric biosensing component. MNs extracted ISF through negative pressure, which was then guided by microchannels to a reaction chamber. The biosensor component used a double-antibody sandwich based on ELISA for C-peptide detection, with regeneration for 10 assays. The mobile app detected the color change and then provided the related C-peptide concentration value.[95] SERS has also been used to analyze the biomarker in the collected skin ISF. Xiao et al. integrated hollow MNs (4 × 4) for skin ISF extraction with a microfluid chip for fluid transport and storage under a negative pressure from a suction cup (Fig. 6A–C). A 3D gold nanoarray SERS substrate embedded within the microfluidic chamber enabled label-free Raman detection of uric acid (Fig. 6D). When coupled with a handheld Raman spectrometer, the device achieved rapid, portable, and ultrasensitive uric acid monitoring with a detection limit of 0.51 μM.[96] Electrochemical biosensors are also frequently used as the off-tip sensing component, which can be part of a circuit board (PCB) containing wireless communication components.[97] For example, Abbasiasl et al. developed a wearable touch-activated device integrating polycarbonate hollow MNs, a microfluidic chip, and wireless communication elements.[98] The microfluidic chip collected the ISF from MNs with the assistance of vacuum and guided the liquid to the sensing components. The wireless communication component enabled real-time data transmission to a mobile app, supporting continuous glucose and pH monitoring.[98]

3.3 MN wearable devices with on-tip sensors

On-tip biosensing works through the on-tip incorporated recognition assay which generates colorimetric, fluorescent, and SERS signals. Detection can be achieved through simple visual inspection or portable devices. For example, He et al. designed a colorimetric HA MN tattoo with segmented areas for multiplexed detection. Each area had specific reagents loaded, forming dermal tattoos upon skin insertion through tip dissolution. The design ensured >85% pattern fidelity for the simultaneous detection of pH, glucose, uric acid, and temperature through distinct color changes, readable by the naked eye or a camera.[99] Researchers also developed a wearable fluorescence-based MN sensor array for continuous glucose monitoring.[100] The array consisted of silk fibroin MNs that had glucose-responsive fluorescent monomers with diboronic acid (glucose-binding) and anthracene (fluorescence) moieties. Anthracene fluorescence was quenched at low glucose levels, while the binding of glucose restored the fluorescence. The fluorescence output was conveniently detected using a smartphone app,
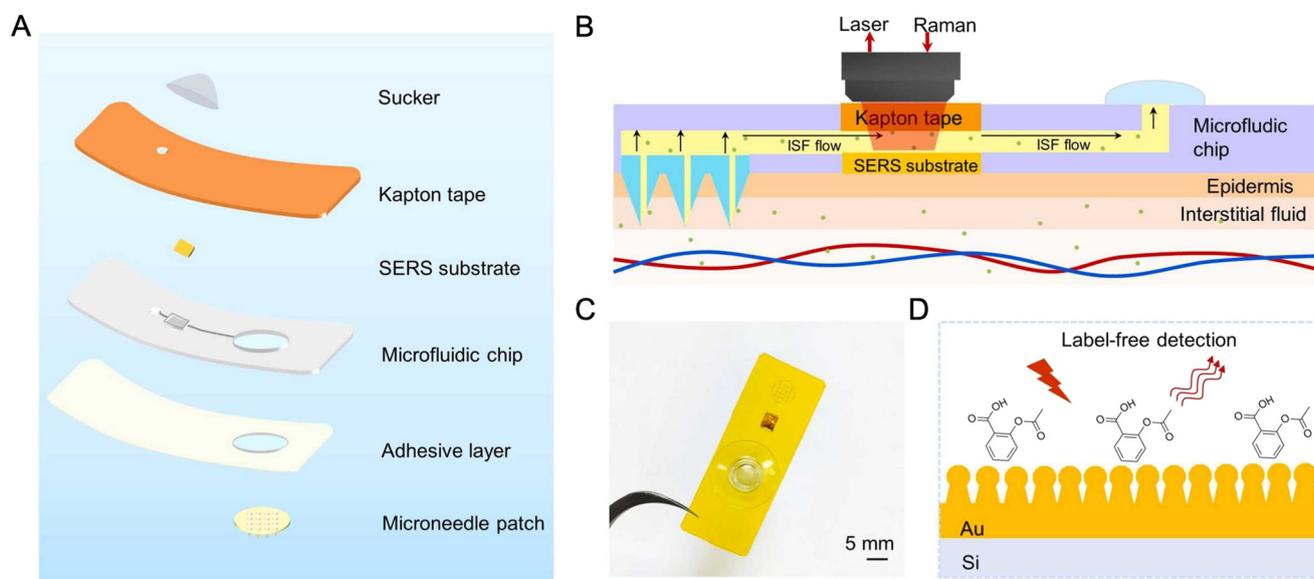
Fig. 6 MN wearable devices with off-tip sensors for uric acid monitoring: (A) the design of the wearable MN sensor integrating hollow MNs, a microfluidic chip, and SERS substrate. (B) Skin ISF sampling and sensing of the wearable off-tip MN sensor. (C) The image of the integrated wearable MN device. (D) The uric acid-sensing on the SERS substrate. Reproduced with permission from ref. 96. Copyright 2023, Elsevier.

facilitating tether-free glucose monitoring with enhanced patient mobility.[100]

On-tip biosensors can also be electrochemical and generate continuous readout of electrical signals.[101,102] In these devices, the MN array serves as the working, reference, and/or counter electrodes in a two- or three-electrode system. Zhang et al. designed a wearable MN sensor device where each electrode (working, reference, and counter) was an individual MN array patch (10×10).[103] MNs were designed in a core–shell structure with a silver paste core and an enzyme-incorporated hydrogel layer. The three-MN-patch sensor was then incorporated with PCB to allow real-time ISF glucose monitoring from a mobile phone through wireless communication.[103] To minimize the size of wearable devices, fewer needles could be used for each individual electrode. For example, two 3-electrode systems (each with 6 working MN electrodes, 8 counter MN electrodes, and 1 reference MN electrode) for multiplexed sensing achieved a high degree of miniaturization and were fully integrated with a compact 5.3 cm^2 PCB.[104] This multiplexed sensing can be extended for sensing more analytes by using a single MN as the working electrode for single-analyte sensing. For example, Li et al. developed a self-calibrating multiplexed MN electrode array, where each electrode was a single MN (Fig. 7A). It could detect 9 analytes (glucose, cholesterol, uric acid, lactate, ROS, Na$^+$, K$^+$, Ca^{2+}, pH) in ISF with self-calibration.[105] If further miniaturization is required, different electrodes can be placed on one single MN tip.[106] Yang et al. developed a wearable device with one MN tip containing four electrodes (two working, one reference, one counter) (Fig. 7B). This device simultaneously monitored glucose and metformin in ISF through differential pulse voltammetry (DPV) with a smartphone app for real-time analysis. This would enable personalized diabetes treatment through PK/PD evaluation.[106] Finally, different electrochemical and physical sensors can be integrated into the same device. Chang et al. developed a hybrid flexible wristband with an MN sensor to analyze the ISF biomarkers, an ultrasonic transducer for blood pressure monitoring, and a biopotential electrode for ECG monitoring. The combination of these systems provided a comprehensive mapping of metabolic and cardiovascular functions simultaneously.[107]
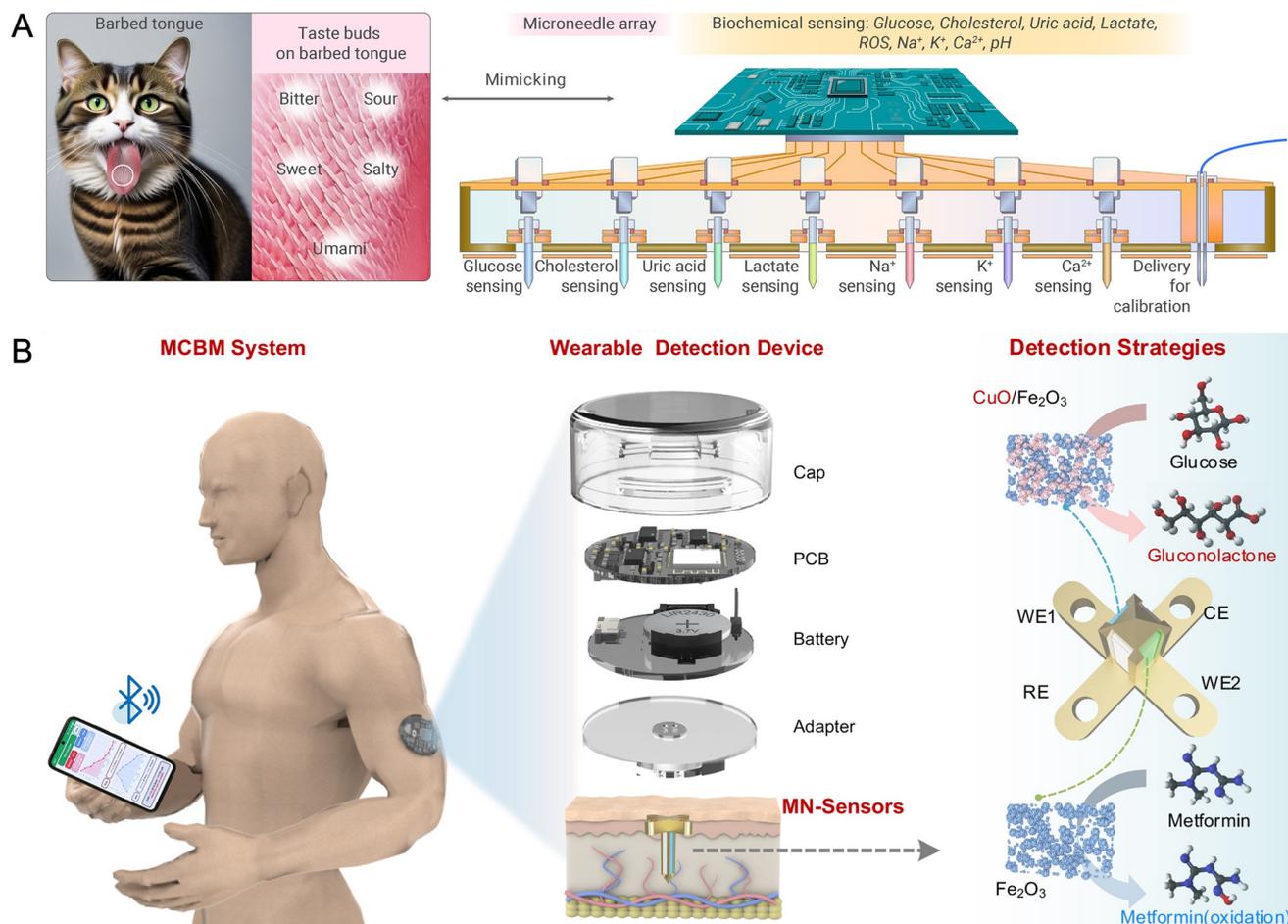

Fig. 7 MN wearable devices with on-tip sensors: (A) self-calibrating multiplexed MN electrode array, in which each electrode is a single MN, enabling detection of nine analytes in ISF (glucose, cholesterol, uric acid, lactate, ROS, Na$^+$, K$^+$, Ca^{2+}, and pH). Reproduced with permission from ref. 105. Copyright 2025, Elsevier. (B) Wearable device with one single MN containing four electrodes (two working, one reference, one counter). Reproduced from ref. 106 under the CC-BY-NC-ND license.

3.4 Commercialized MN wearable devices

The most known products are devices for continuous glucose monitoring (CGM). They are class II medical devices under the FDA regulation section of integrated continuous glucose monitoring system (21 CFR 862.1355) or glucose test system (21 CFR 862.1345). CGM systems, such as the Abbott FreeStyle Libre 3 Plus and Dexcom G7, comprise two main components: a sensor module and a sensor applicator. Within the applicator, retractable hollow stainless-steel MNs are pre-loaded and serve to insert the sensor filament beneath the skin. After insertion, the needle automatically retracts, leaving the thin and flexible sensing filament in the interstitial space to access ISF. The sensing filament differs slightly between systems: the FreeStyle Libre 3 Plus employs a polymer-based filament, whereas the Dexcom G7 utilizes a platinum and tantalum core wire. In both designs, the filament tip lies in an enzyme-based electrochemical sensor, where glucose oxidase catalyzes the oxidation of glucose, generating hydrogen peroxide that is subsequently oxidized at the working electrode. The resulting current is proportional to local glucose concentration, enabling continuous, real-time glucose monitoring. Data are then transmitted *via* near-field communication and Bluetooth, enabling real-time display of glucose readings, trends, and customizable alerts.

The Biolinq Shine Autonomous Time-in-Range Microsensor has been recently granted classification as a prescription class II medical device by the FDA under the regulation of glucose range monitoring system (21 CFR 862.1359). Unlike the Abbott FreeStyle Libre 3 Plus and Dexcom G7 using filament sensing strategy, it integrates an array of MN sensors that reside in the intradermal layer to access interstitial fluid glucose, eliminating the need for retractable subcutaneous introducer needles. Its MN sensor array works in conjunction with an accelerometer and ambient light sensor to measure and record physiological data. Different from quantitative CGMs, it features a qualitative color-changing indicator light that output glucose level trends continuously, while a paired mobile app provides more granular glucose information and correlates it with meals, rest, and activity levels. This device is designed for adults aged 22 and older who do not use insulin. It supports lifestyle and behavioral modifications for glycemic control but cannot make acute medical decisions such as insulin dosing or medication adjustments.

4. MN wearable devices for monitoring electrophysiological signals

4.1 Design of MN electrodes

As electrodes for electrophysiological signal transduction, including EEG, ECG, EMG, and ENoG, MNs rely on their conductive properties. In contrast to conventional wet electrodes and flat dry electrodes, MN-based electrophysiological monitoring electrodes increase the skin contact area, reducing signal noises and improving the quality of the acquired signals. Solid MNs and multilayer coated MNs are popular choices with innovations in improving the skin adhesion, MN conductivity, and MN patch flexibility.[108] One example is a titanium-coated barbed MN array electrode using photolithography and PDMS thermal expansion. These MN electrodes could record high-quality ECG in static/dynamic states with lower impedance and higher amplitude than Ag/AgCl electrodes. The barbed structure also enhanced skin adhesion, with 3.3 times higher pull-out force than barbless ones (Fig. 8A).[108]

Metallic materials like stainless steel,[109] gold, and silver[110,111] are commonly used as the conductive substrate or layer of MN electrodes. Krieger *et al.* fabricated dry MN electrodes using medical-grade stainless steel through direct metal laser sintering. Compared to needle-free electrodes, electrode–skin contact impedance was reduced by approximately 63%.[109] Gold or silver is typically deposited onto solid MNs made from material substrate like silicon,[112] polyimide,[100,113] epoxy,[114] *etc.* to enable electrical signal conduction, which can enhance the mechanical strength to facilitate efficient skin penetration. Conductive polymers, such as poly(3,4-ethylenedioxythiophene) (PEDOT) and PPy[113,115,116] were also used for the coating of solid MNs. For instance, Zhou *et al.* introduced modulus-adjustable and mechanically adaptive dry MN electrodes from PEDOT:PSS. The MN electrodes enabled high-quality EMG, ECG, EEG, and ECoG recordings, with better long-term stability than Ag/AgCl electrodes (Fig. 8B).[115] MN electrodes could also be coated with conductive 2D materials, such as MXene.[117,118] Chen *et al.* developed MXene-based MN electrodes for brain–computer interface with low impedance and high-quality EEG recording.[117]

The use of flexible substrate materials together with structural designs would allow MN electrodes to conform to different surface curvatures. Conductive fabrics, in particular, are commonly used as the base for MN electrodes due to their electrical conductivity. Singh *et al.* developed flexible conductive fabric-backed MN electrodes that acquired high-quality ECG and EMG signals without the need of wet gel or skin shaving. The conductive fabric was a nylon ripstop fabric covered by nickel, copper, silver, and a waterproof layer, providing flexibility to conform to body curves.[114] Another choice is polymer, such as the hybrid of silk fibroin and polyurethane.[110] The incorporation of metal serpentine interconnection configuration on polymer substrate allows the metal traces to stretch and bend without fracturing. For example, a highly flexible and stretchable MN electrode array has been developed by combining gold serpentine interconnects and elastomeric silicone substrate. This material allowed the MN array to conform to soft tissues while providing a stable interface,[119] thus achieving high-quality intramuscular EMG recording and better localized sensing than planar electrodes. Moreover, the flexibility of the MN electrode substrate is adjustable through surface structure modifications, such as mesh patterns[120] and Miura-ori.[121] Hou *et al.*
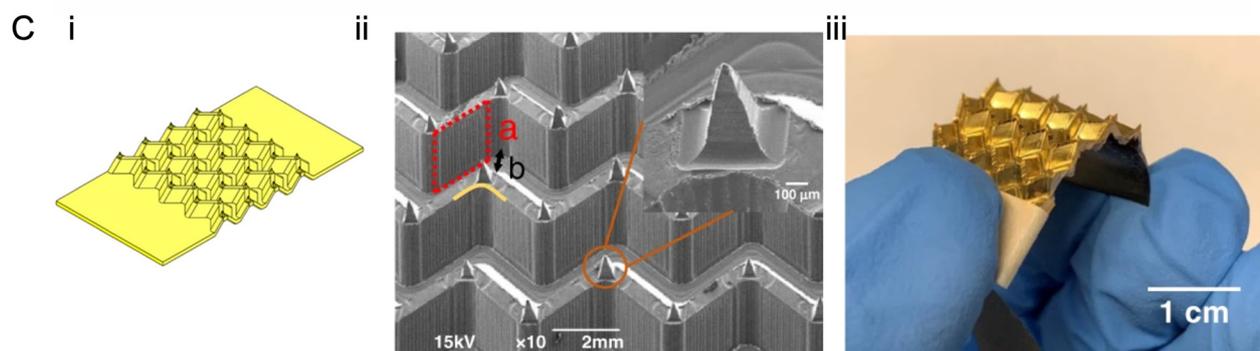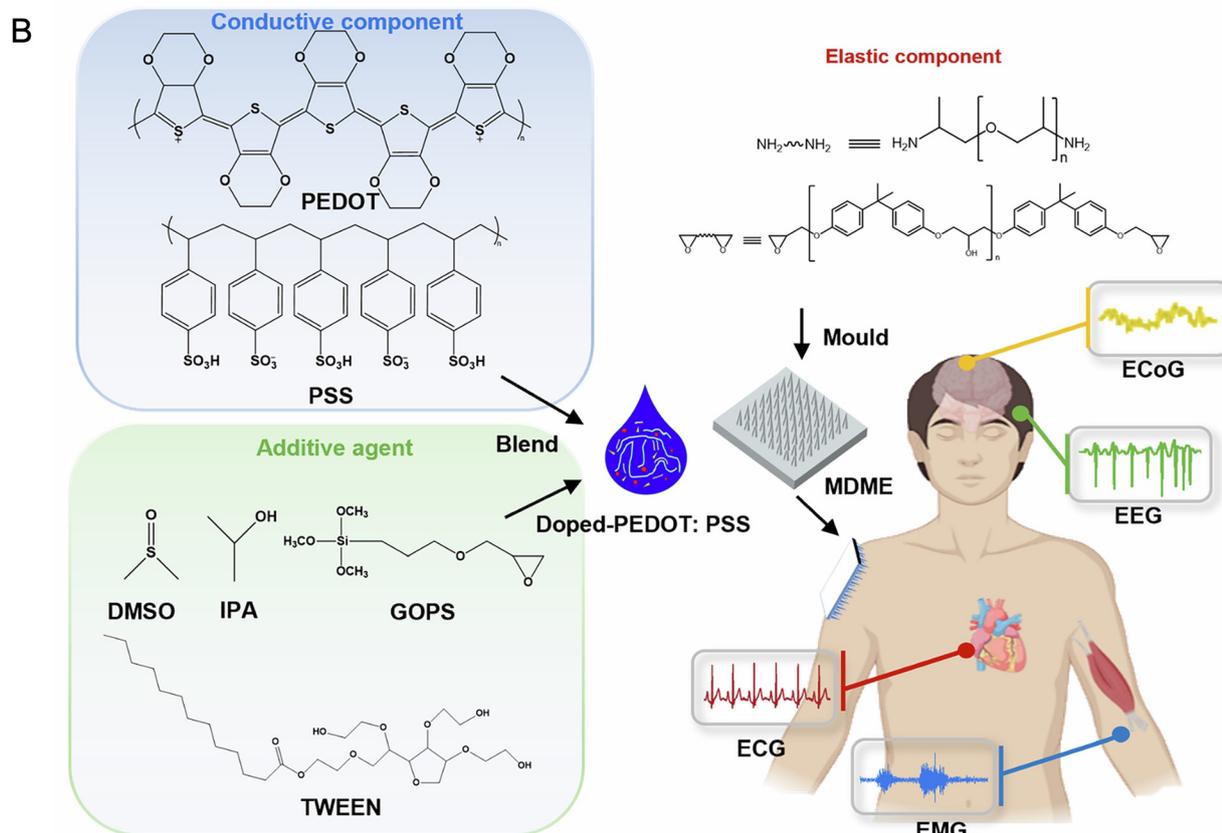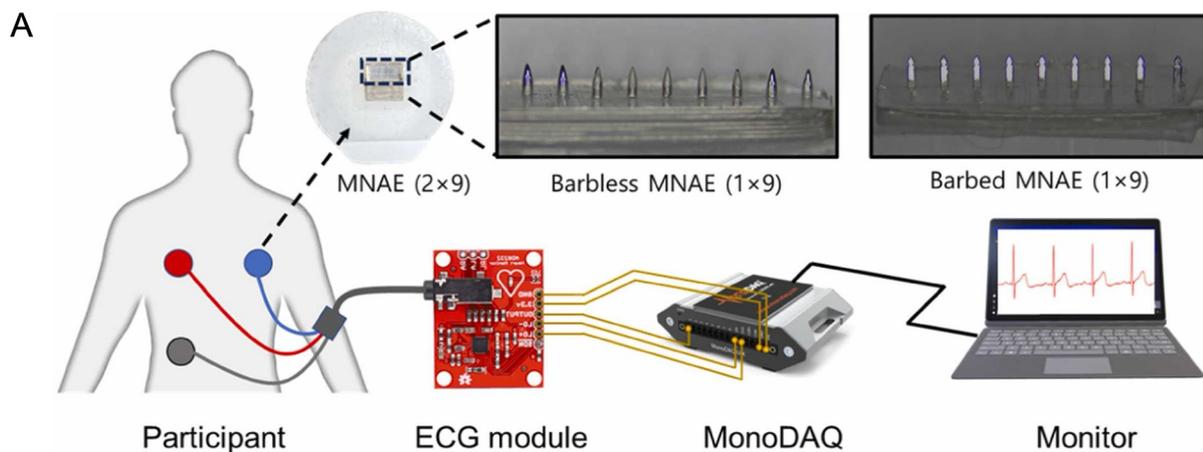
Fig. 8 MN electrodes for electrophysiological signal monitoring. (A) Barbed MN array electrode enhancing skin adhesion for ECG monitoring. Reproduced with permission from ref. 108. Copyright 2024, Elsevier. (B) Conductive MNs made from PEDOT:PSS for EMG, ECG, EEG, and ECoG recording. Reproduced from ref. 115 under the CC-BY-NC-ND 4.0 license. (C) (i) Illustration of the Miura-ori structured MN array electrode; (ii) SEM structure of Miura-ori structured MN array; (iii) flexibility of the MN electrode. Reproduced from ref. 121 under the CC-BY 4.0 license.

developed a Miura-ori-structured MN array electrode with two-directional in-plane bendability (Fig. 8C, i and ii). This unique structure not only enhanced mechanical flexibility but also mitigated metal layer peeling (Fig. 8C, iii).[121]

Fig. 9 MN wearable devices for electrophysiological signal monitoring. (A) Integration of MN electrodes with flexible electronics for facial biosensing: (i) illustration of a soft wearable electronic mask for facial EMG monitoring; (ii) design of the electrode component and PCB module. Reproduced from ref. 122 under the CC-BY 4.0 license. (B) Integration of MN electrodes as brain–computer interfaces with an EEG scalp cap: (i) Mxene MN electrode as a brain–computer interface; (ii) the wearable EEG cap. Reproduced with permission from ref. 117. Copyright 2025, American Chemical Society. (C) Integration of MN electrode devices with artificial neural networks for enhanced bioelectrical signal interpretation: (i) wearable EMG sensor for real-time monitoring of EMG signals; (ii) original and stretched wearable EMG sensor; (iii) gesture recognition by a graph neural network using transmitted data from the EMG sensor. Reproduced from ref. 126 under the CC-BY 4.0 license.

4.2 The integration of MN electrodes into wearable devices

MN electrodes can be integrated with flexible electronics into wearable devices to monitor electrophysiological signals.[112,122–124] For example, Li et al. created a wearable wireless system by adding polyimide-based flexible MN array electrodes to flexible printed circuits.[113] The system connected MN electrodes to front-end amplifiers, microcontrollers with Bluetooth, and power modules. Simultaneous recording of multiple physiological signals like ECG, EMG, EOG, and EEG was accomplished with low motion artifacts.[113] Another example is a wireless facial biosensing system with flexible MN electrodes in a soft and wearable electronic mask (Biomask) (Fig. 9A i). This system provided facial EMG monitoring with real-time data transmission by a PCB module (Fig. 9A ii), supporting facial palsy assessment, intraoperative nerve monitoring, and long-term follow-up.[122]

The wearable devices with MN electrodes can also serve as a human–machine interface or brain–computer interface for seamless interactions between the human body and external devices.[115,117,120,125] For instance, Kim et al. developed a wearable wireless system combining a stretchable MN adhesive patch with a flexible circuit for adaptability to skin deformation.[125] It had a closed-loop control of exoskeleton robots, where the MN patch on lower limb muscles transmitted EMG signals wirelessly, and triggered assistance when signals exceeded the thresholds. The system reduced back muscle activation by 18.1% during lifting, showing robust performance in both pretreated and perspiring skin conditions, advancing human–machine interfaces. Additionally, these MN devices can function as a brain–computer interface[115,117,120] for facilitating direct communication between the brain and computers. Detecting and interpreting neural signals through MN electrodes is promising for bridging the gap between human neural activity and digital systems. For example, a brain–computer interface framework has been integrated with MXene MN electrodes into wearable EEG cap devices (Fig. 9B, i and ii). The 1 mm^2 dry MN electrodes penetrated the epidermis, delivering stable performance in vibrational and motion scenarios.[117]

To enhance the interpretation of bioelectrical signals, the MN wearable devices can incorporate with artificial neural networks. Lee et al. presented a stretchable array of bipolar sEMG electrodes with a self-attention-based graph neural network for gesture recognition (Fig. 9C, i).[126] A sticky, hole-patterned patch provided skin-like stretchability and water vapor permeability for stable signal delivery (Fig. 9C, ii). It aimed to spatially cover skeletal muscles and acquire regional EMG activity data from 18 static and dynamic gestures, achieving ~97% accuracy with one trial per gesture (Fig. 9C, iii). Notably, it retained ~95% accuracy over 72 h of long-term testing and after 10 reuses, showing promise for applications in prosthetic control and smart device interaction.[126] Finally, MN wearable devices can integrate with virtual reality (VR) technology. Mahmood et al. developed a wireless soft scalp electronic system with flexible

EEG MN electrodes and a wireless electronic circuit as the brain–computer interface.[127] A convolutional neural network was used to preprocess and classify the motor imagery brain signals delivered by the scalp device. The wearable scalp device was subsequently integrated with VR which provides visual cues in the form of animated limbs and instant feedback. This setup allows users to control a VR game using imagined movements through the brain–computer interface, while the VR component enhances task visualization and improves classification accuracy.[127]

5. Challenges and future perspectives for MN-based wearable devices

5.1 Technical challenges

Reliable and consistent biofluid sampling. Reliable and consistent sampling of biofluids, particularly skin ISF, remains a significant technical hurdle.[128] Specifically, skin hydration dynamically modulates the mechanical properties (e.g., stiffness, elasticity) of the stratum corneum, leading to interindividual and intraindividual variations in MN penetration and sampling depth. Skin hydration status also affects the passive flow of ISF into MNs: dehydrated skin results in insufficient ISF volume, while over-hydration induces ISF dilution, both undermining the consistency of target biomarker quantification. Notably, the accurate quantification of extracted biofluid volume remains a critical challenge, often leading to unreliable biomarker concentration calculations. To address the problems, recent strategies have focused on developing MN applicators for standard deployment and incorporating compact microfluidic chips integrated with micropumps or vacuum-driven modules on MN patches for active biofluid sampling.[58,129] Despite these advances, a smart integrated deployment system is needed that synergizes skin hydration sensors to real-time assess skin water content, adaptive adjustments of MN penetration depth control, and a biofluid microfluidic reservoir for quantitative collection.

Sensor efficiency, stability, and durability. The efficiency and stability of MN-based biosensors directly affect long-term performance. Although bioreceptor (e.g., enzymes, antibodies, and aptamers) immobilized MN biosensors perform sensitive and selective biosensing, they often suffer from limited shelf life due to bioreceptor degradation/denaturation and biofouling during extended wear.[130] These factors critically undermine biosensor efficiency and stability, thereby compromising durability and repeatability. For physical sensors, interface mismatch between rigid modules and flexible MN arrays reduces signal fidelity over time. Additionally, sensor durability is a key factor for cost-effectiveness in field deployment. Disposable devices avoid durability issues but increase long-term costs. Proposed improvement strategies include hydrophilic/anti-biofouling coatings (e.g., chitosan and Nafion) to prolong bioreceptor activity, self-healing conductive hydrogels for mechanical fatigue resistance, and semi-disposable designs (reusable

modules and replaceable MN patches) to balance durability and cost.[130]

Flexible electronic integration. Merging MN biosensors with on-board microelectronics poses its own challenges. A wearable wireless MN device should embed analog front-end electronics, analog-to-digital conversion, power sources, and wireless communication. Conventional rigid silicon chips and coin-cell batteries are stiff, bulky, and uncomfortable for prolonged wear, while flexible electronics (*e.g.*, organic thin-film transistors and stretchable antennas) still face challenges in durability and integration density. It is still a complex procedure to seamlessly integrate batteries or energy harvesters, radio transmitters, and signal-conditioning circuits into a thin flexible device.[131] Hybrid integration strategies (like layer-by-layer lamination and 3D printed interconnections) have shown promise for reducing bulk, but scalability remains limited.[132]

5.2 Clinical validation

The clinical validation of MN-based measurements faces hurdles. In particular, the relationship between disease biomarkers in skin ISF and in blood has not been fully established.[133] Frequent or large volumes of ISF sampling can disturb the local microenvironment and even trigger immune effects, making ISF concentrations diverge from blood levels.[15] As a result, there could be diagnostic inaccuracies when detecting a target analyte with a MN sensor. Comprehensive comparative studies are therefore necessary. Long-term *in vivo* trials in diverse groups of people, including different ages, skin types, and health conditions, are needed to link biomarker levels in ISF with those in blood, using standard laboratory methods such as LC-MS/MS or ELISA.

5.3 Industrialization and regulatory challenges

Scalable manufacturing and cost considerations. The cost and large-scale production of MN biosensors depend not only on how the MNs themselves are made but also on how easily they can be combined with electronic components. Currently, MN manufacturing technologies including micromolding, photolithography, 3D printing, and droplet-born air blowing.[134] Among these methods, micromolding using biocompatible polymers already enable low-cost, high-speed fabrication of MN arrays, making them suitable for mass production.[23] However, the main cost lies in the post-fabrication integration of sensing component and microelectronics, which requires multi-step assembly processes and micron-level alignment that are difficult to scale. As a result, fully integrated MN biosensors remain expensive. For context, commercially available CGMs, such as the Abbott FreeStyle Libre 3 Plus, achieve a price of around $100 per sensor for 15 days of use by using highly optimized, single-use designs with simplified electronics. To close this gap, emerging hybrid manufacturing strategies, such as combining inkjet or screen printing of conductive traces with

insert molding of MN arrays,[132] could streamline device assembly, reduce alignment complexity, and ultimately lower production costs.

Regional regulatory. MN biosensing wearable devices, as minimally invasive medical devices, face distinct regulatory frameworks across regions. In the United States, the FDA classifies most diagnostic MN wearables into class II and follow the 510(k) premarket notification pathway. CGM, like Abbott's FreeStyle Libre 3 and Dexcom G7, have secured FDA clearance under the regulation of integrated continuous glucose monitoring system (21 CFR 862.1355) or glucose test system (21 CFR 862.1345). In contrast, the novel MN sensing platform, the Biolinq Shine Autonomous Time-in-Range Microsensor, has been recently granted classification as a prescription class II medical device by the FDA under the regulation of glucose range monitoring system (21 CFR 862.1359). In China, CGM devices are classified as class III medical devices by the National Medical Products Administration (NMPA), requiring rigorous premarket approval. The clinical evaluation for CGM cannot be exempted. Manufacturers are required to provide clinical performance data demonstrating safety and effectiveness in target populations (*e.g.*, insulin-treated patients or those with gestational diabetes). However, China has not approved any MN-based monitoring device similar to Biolinq Shine yet. In the European Economic Area (EEA), MN wearables are governed by the Medical Device Regulation (MDR) and require CE marking for commercialization. Most diagnostic MN devices are classified as class IIa or IIb, with approval contingent on compiling comprehensive technical documentation, risk assessments, and clinical evaluation reports. Such regional variations in marketing policies significantly affect time to market, reimbursement eligibility, and global scalability, necessitating early engagement with regulatory bodies during device development.

5.4 Future outlook: intelligent MN platforms

An ideal MN wearable system would continuously monitor biomarkers or electrophysiological signals and provide alerts/suggestions for the timely intervention of health conditions (Fig. 10).[135] Progress toward this vision has already been demonstrated in prototype devices.[136,137] For example, one recent study developed a wearable closed-loop system for diabetes in which an MN-based glucose sensor was integrated with an iontophoretic insulin delivery module.[136] This device detected rising glucose levels in real time and immediately triggered a proportional insulin release, maintaining normoglycemia in diabetic rats. In principle, multi-analyte MN arrays (*e.g.* for lactate, electrolytes, stress hormones) could feed into a feedback controller that actuates a micro-reservoir or patch injector. This self-regulating architecture, combining sensing, electronics, and drug delivery in a single skin-conformal platform, could revolutionize chronic disease management by providing on-demand therapy without user intervention. The emergence of
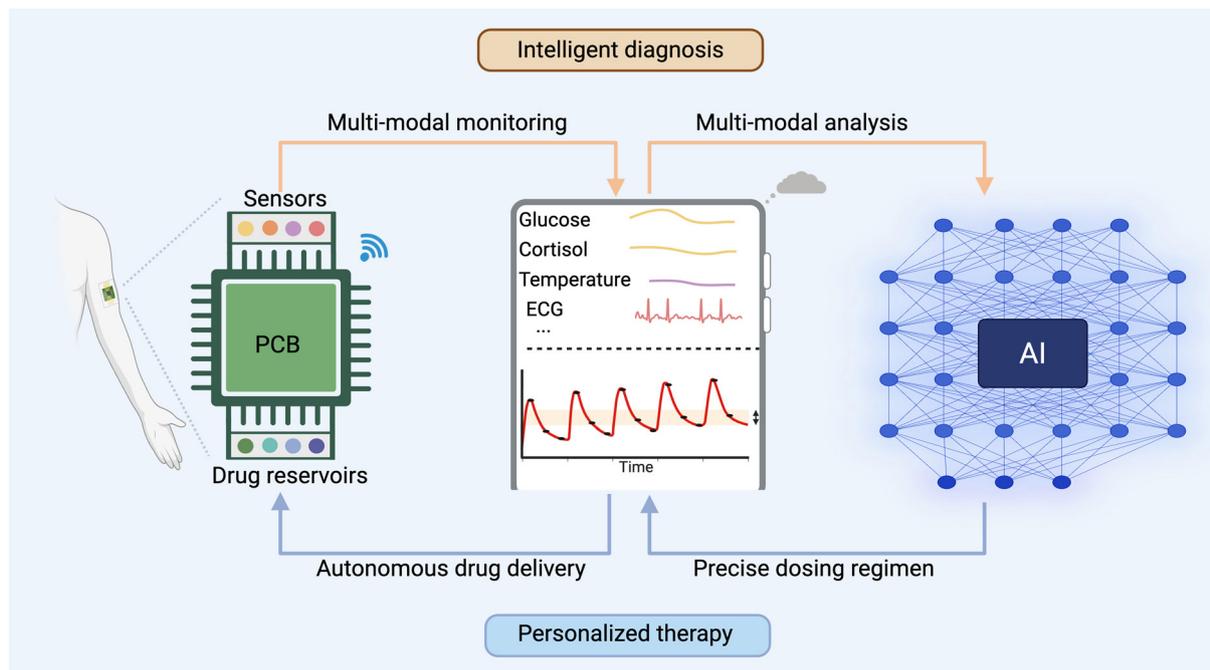
Fig. 10 The ideal MN wearable devices for personalized medicine. Created with https://BioRender.com.

AI can further facilitate the realization of the ideal MN devices.[135] AI and machine-learning algorithms can process the continuous streams of multi-modal data from a MN device to identify trends and forecast events.[131] For instance, subtle patterns in glucose and movement data could be recognized weeks in advance of a metabolic crisis, prompting pre-emptive dietary or insulin-dosing advice. Moreover, AI-driven platforms can translate raw sensor outputs into individualized recommendations. There could be an analogous to fitness wearables that suggest hydration and activity changes, or an AI-enhanced MN patch that could advise users when to eat, take medications, or seek care based on their unique physiology. In addition, data-driven algorithms can compensate for signal artefacts and inter-subject variability. By filtering motion noise or adaptively recalibrating sensor baselines, readouts could be stabilized over time.

Conflicts of interest

There are no conflicts of interest to declare.

Data availability

No primary research results, software, or code are included in this article, and no new data were generated or analysed in the preparation of this review.

Acknowledgements

References

1 Y. Wang, H. Haick, S. Guo, C. Wang, S. Lee, T. Yokota and T. Someya, *Chem. Soc. Rev.*, 2022, **51**, 3759–3793.

2 S. M. A. Iqbal, I. Mahgoub, E. Du, M. A. Leavitt and W. Asghar, *npj Flexible Electron.*, 2021, **5**, 9.

3 A. Keshet, L. Reicher, N. Bar and E. Segal, *Nat. Metab.*, 2023, **5**, 563–571.

4 Z. Wang, Y.-c. Lai, Y.-t. Chiang, J. M. Scheiger, S. Li, Z. Dong, Q. Cai, S. Liu, S.-h. Hsu, C.-c. Chou and P. A. Levkin, *ACS Appl. Mater. Interfaces*, 2022, **14**, 50152–50162.

5 Z. Wang, Q. Cai, L. Lu and P. A. Levkin, *Small*, 2024, **20**, 2305214.

6 T. S. Vo and K. Kim, *Adv. Intell. Syst.*, 2024, **6**, 2300730.

7 J. Li, H. Chu, Z. Chen, C. K. Yiu, Q. a. Qu, Z. Li and X. Yu, *ACS Nano*, 2024, **18**, 17407–17438.

8 K. M. Clark and T. R. Ray, *ACS Sens.*, 2023, **8**, 3606–3622.

9 F. Gao, C. Liu, L. Zhang, T. Liu, Z. Wang, Z. Song, H. Cai, Z. Fang, J. Chen, J. Wang, M. Han, J. Wang, K. Lin, R. Wang, M. Li, Q. Mei, X. Ma, S. Liang, G. Gou and N. Xue, *Microsyst. Nanoeng.*, 2023, **9**, 1.

10 H. Li, S. Gu, Q. Zhang, E. Song, T. Kuang, F. Chen, X. Yu and L. Chang, *Nanoscale*, 2021, **13**, 3436–3453.

11 M. S. Li, H. L. Wong, Y. L. Ip, Z. Peng, R. Yiu, H. Yuan, J. K. Wai Wong and Y. K. Chan, *ACS Sens.*, 2022, **7**, 1300–1314.

12 H.-R. Lim, S. M. Lee, S. Park, C. Choi, H. Kim, J. Kim, M. Mahmood, Y. Lee, J.-H. Kim and W.-H. Yeo, *Biosens. Bioelectron.*, 2022, **210**, 114329.

13 Z. Wang, Z. Lin, X. Mei, L. Cai, K.-C. Lin, J. F. Rodríguez, Z. Ye, X. S. Parraguez, E. M. Guajardo, P. C. García Luna, J. Y. J. Zhang and Y. S. Zhang, *Adv. Mater.*, 2025, **37**, 2416260.

14 T. Saha, S. Mukherjee, M. D. Dickey and O. D. Velev, *Lab Chip*, 2024, **24**, 1244–1265.

15 Z. Wu, Z. Qiao, S. Chen, S. Fan, Y. Liu, J. Qi and C. T. Lim, *Commun. Mater.*, 2024, **5**, 33.

16 D. Sim, M. C. Brothers, J. M. Slocik, A. E. Islam, B. Maruyama, C. C. Grigsby, R. R. Naik and S. S. Kim, *Adv. Sci.*, 2022, **9**, 2104426.

17 M. Friedel, I. A. P. Thompson, G. Kasting, R. Polsky, D. Cunningham, H. T. Soh and J. Heikenfeld, *Nat. Biomed. Eng.*, 2023, **7**, 1541–1555.

18 C. Merzougui, X. Yang, D. Meng, Y. Huang and X. Zhao, *Adv. Healthcare Mater.*, 2025, **14**, 2404420.

19 J. Yang, H. Zhang, T. Hu, C. Xu, L. Jiang, Y. Shrike Zhang and M. Xie, *Chem. Eng. J.*, 2021, **426**, 130561.

20 M. Zheng, T. Sheng, J. Yu, Z. Gu and C. Xu, *Nat. Rev. Bioeng.*, 2024, **2**, 324–342.

21 N. Xu, W. Xu, M. Zhang, J. Yu, G. Ling and P. Zhang, *Adv. Mater. Technol.*, 2022, **7**, 2101595.

22 G. Kim, H. Ahn, J. Chaj Ulloa and W. Gao, *Med-X*, 2024, **2**, 15.

23 J. Li, M. Wei and B. Gao, *ACS Sens.*, 2024, **9**, 1149–1161.

24 L. K. Vora, A. H. Sabri, P. E. McKenna, A. Himawan, A. R. J. Hutton, U. Detamornrat, A. J. Paredes, E. Larrañeta and R. F. Donnelly, *Nat. Rev. Bioeng.*, 2024, **2**, 64–81.

25 Y. Hu, E. Chatzilakou, Z. Pan, G. Traverso and A. K. Yetisen, *Adv. Sci.*, 2024, **11**, 2306560.

26 T. Hu, K. S. Lui, E. B. Ko, Y. Zhao, Q. Zhang, H. Yang, M. Zheng, H. Chang, B. Guo, A. K. L. Cheung and C. Xu, *Matter*, 2025, **8**, 102038.

27 X. Jiang, E. C. Wilkirson, A. O. Bailey, W. K. Russell and P. B. Lillehoj, *Cell Rep. Phys. Sci.*, 2024, **5**, 101975.

28 C. Kolluru, M. Williams, J. S. Yeh, R. K. Noel, J. Knaack and M. R. Prausnitz, *Biomed. Microdevices*, 2019, **21**, 14.

29 P. P. Samant, M. M. Niedzwiecki, N. Raviele, V. Tran, J. Mena-Lapaix, D. I. Walker, E. I. Felner, D. P. Jones, G. W. Miller and M. R. Prausnitz, *Sci. Transl. Med.*, 2020, **12**, eaaw0285.

30 C. Kolluru, R. Gupta, Q. Jiang, M. Williams, H. Gholami Derami, S. Cao, R. K. Noel, S. Singamaneni and M. R. Prausnitz, *ACS Sens.*, 2019, **4**, 1569–1576.

31 S. Kim, M. S. Lee, H. S. Yang and J. H. Jung, *Sci. Rep.*, 2021, **11**, 14018.

32 A. H. Hung, N. U. Rajesh, A. Bermudez, S. M. Boczek, F. J. Garcia-Marqués, Y. L. Tan, J. Hwang, P. D. Sinawang, D. Ilyin, G. B. Jacobson, U. Demirci, S. P. Poplack, S. J. Pitteri and J. M. DeSimone, *bioRxiv*, 2025, DOI: 10.1101/2025.03.13.641882.

33 N. Zoratto, D. Klein-Cerrejon, D. Gao, T. Inchiparambil, D. Sachs, Z. Luo and J. C. Leroux, *Adv. Sci.*, 2024, **11**, e2308809.

34 G. Wang, Y. Zhang, H. K. Kwong, M. Zheng, J. Wu, C. Cui, K. W. Y. Chan, C. Xu and T.-H. Chen, *Adv. Sci.*, 2024, **11**, 2306188.

35 M. Zheng, Y. Zhang, T. Hu and C. Xu, *Bioeng. Transl. Med.*, 2023, **8**, e10413.

36 M. Zheng, Z. Wang, H. Chang, L. Wang, S. W. T. Chew, D. C. S. Lio, M. Cui, L. Liu, B. C. K. Tee and C. Xu, *Adv. Healthcare Mater.*, 2020, **9**, 1901683.

37 H. Chang, M. Zheng, X. Yu, A. Than, R. Z. Seeni, R. Kang, J. Tian, D. P. Khanh, L. Liu, P. Chen and C. Xu, *Adv. Mater.*, 2017, **29**, 1702243.

38 Y. Dai, J. Nolan, E. Madsen, M. Fratus, J. Lee, J. Zhang, J. Lim, S. Hong, M. A. Alam, J. C. Linnes, H. Lee and C. H. Lee, *ACS Appl. Mater. Interfaces*, 2023, **15**, 56760–56773.

39 J. Zhu, X. Zhou, H.-J. Kim, M. Qu, X. Jiang, K. Lee, L. Ren, Q. Wu, C. Wang, X. Zhu, P. Tebon, S. Zhang, J. Lee, N. Ashammakhi, S. Ahadian, M. R. Dokmeci, Z. Gu, W. Sun and A. Khademhosseini, *Small*, 2020, **16**, 1905910.

40 K. M. Saifullah, A. Mushtaq, P. Azarikhah, P. D. Prewett, G. J. Davies and Z. Faraji Rad, *Microsyst. Nanoeng.*, 2025, **11**, 3.

41 K. M. Saifullah, P. Azarikhah and Z. Faraji Rad, *Mater. Today Chem.*, 2025, **45**, 102661.

42 N. Xu, M. Zhang, W. Xu, G. Ling, J. Yu and P. Zhang, *Analyst*, 2022, **147**, 1478–1491.

43 N. G. Oh, S. Y. Hwang and Y. H. Na, *ACS Omega*, 2022, **7**, 25179–25185.

44 C. G. Li, M. Dangol, C. Y. Lee, M. Jang and H. Jung, *Lab Chip*, 2015, **15**, 382–390.

45 P. R. Miller, R. M. Taylor, B. Q. Tran, G. Boyd, T. Glaros, V. H. Chavez, R. Krishnakumar, A. Sinha, K. Poorey, K. P. Williams, S. S. Branda, J. T. Baca and R. Polsky, *Commun. Biol.*, 2018, **1**, 173.

46 T. Elias Abi-Ramia Silva, S. Kohler, N. Bartzsch, F. Beuschlein and A. T. Güntner, *Cell Biomater.*, 2025, **1**, 100008.

47 Y. Li, H. Zhang, R. Yang, Y. Laffitte, U. Schmill, W. Hu, M. Kaddoura, E. J. M. Blondeel and B. Cui, *Microsyst. Nanoeng.*, 2019, **5**, 41.

48 P. Liu, H. Du, Z. Wu, H. Wang, J. Tao, L. Zhang and J. Zhu, *J. Mater. Chem. B*, 2021, **9**, 5476–5483.

49 K. Takeuchi, N. Takama, K. Sharma, O. Paul, P. Ruther, T. Suga and B. Kim, *Drug Delivery Transl. Res.*, 2022, **12**, 435–443.

50 G. Zhu, C. Liu, Y. Lu, X. Mo, J. Dong, K. Xu, Y. Huang, C. Chen, X. Lv, X. Yang and X. Zhao, *ACS Appl. Nano Mater.*, 2025, **8**, 7867–7875.

51 X.-Q. You, Q.-Y. He, T.-W. Wu, D.-Y. Huang, Z.-Z. Peng, D.-Y. Chen, Z. Chen and J. Liu, *Microchem. J.*, 2023, **190**, 108570.

52 F. Leng, M. Zheng and C. Xu, *Exploration*, 2021, **1**, 20210109.

53 C. T. Sharkey, A. F. Aroche, I. G. Agusta, H. Nissan, T. Saha, S. Mukherjee, J. S. Twiddy, M. D. Dickey, O. Velev and M. A. Daniele, *Lab Chip*, 2025, **25**, 4577–4587.

54 F. Ribet, A. Bendes, C. Fredolini, M. Dobielewski, M. Böttcher, O. Beck, J. M. Schwenk, G. Stemme and N. Roxhed, *Adv. Healthcare Mater.*, 2023, **12**, 2202564.

55 C. G. Li, K. Lee, C. Y. Lee, M. Dangol and H. Jung, *Adv. Mater.*, 2012, **24**, 4583–4586.

56   Y. Xie, J. He, W. He, T. Iftikhar, C. Zhang, L. Su and X. Zhang, *Adv. Sci.*, 2024, **11**, 2308716.

57   A. Trautmann, G.-L. Roth, B. Nujiqi, T. Walther and R. Hellmann, *Microsyst. Nanoeng.*, 2019, **5**, 6.

58   T. M. Blicharz, P. Gong, B. M. Bunner, L. L. Chu, K. M. Leonard, J. A. Wakefield, R. E. Williams, M. Dadgar, C. A. Tagliabue, R. El Khaja, S. L. Marlin, R. Haghgooie, S. P. Davis, D. E. Chickering and H. Bernstein, *Nat. Biomed. Eng.*, 2018, **2**, 151–157.

59   M. S. F. Hoffman, J. W. McKeage, J. Xu, B. P. Ruddy, P. M. F. Nielsen and A. J. Taberner, *Expert Rev. Med. Devices*, 2023, **20**, 5–16.

60   J. Kang, K. Y. Kim, S. Kim, H. Hong, B.-S. Bae, S.-K. Kang and W. Lee, *Device*, 2023, **1**, 100112.

61   S. A. Ranamukhaarachchi, C. Padeste, M. Dubner, U. O. Hafeli, B. Stoeber and V. J. Cadarso, *Sci. Rep.*, 2016, **6**, 29075.

62   K. Yi, Y. Wang, K. Shi, J. Chi, J. Lyu and Y. Zhao, *Biosens. Bioelectron.*, 2021, **190**, 113404.

63   M. Dervisevic and N. H. Voelcker, *ACS Mater. Lett.*, 2023, **5**, 1851–1858.

64   L. He, Y. Zhou, M. Zhang, M. Chen, Y. Wu, L. Qi, L. Liu, B. Zhang, X. Yang, X. He and K. Wang, *ACS Sens.*, 2024, **9**, 6563–6571.

65   V. Behnam, A. M. McManamen, H. G. Ballard, B. Aldana, M. Tamimi, N. Milosavić, M. N. Stojanović, M. R. Rubin and S. K. Sia, *Angew. Chem., Int. Ed.*, 2025, **64**, e202414871.

66   D. Al Sulaiman, J. Y. H. Chang, N. R. Bennett, H. Topouzi, C. A. Higgins, D. J. Irvine and S. Ladame, *ACS Nano*, 2019, **13**, 9620–9628.

67   B. Ciui, A. Martin, R. K. Mishra, B. Brunetti, T. Nakagawa, T. J. Dawkins, M. Lyu, C. Cristea, R. Sandulescu and J. Wang, *Adv. Healthcare Mater.*, 2018, **7**, 1701264.

68   W. Lee, S.-h. Jeong, Y.-W. Lim, H. Lee, J. Kang, H. Lee, I. Lee, H.-S. Han, S. Kobayashi, M. Tanaka and B.-S. Bae, *Sci. Adv.*, 2021, **7**, eabi6290.

69   X. Zhou, S. Huang, D. Zhang, W. Liu, W. Gao, Y. Xue and L. Shang, *Anal. Chem.*, 2023, **95**, 12104–12112.

70   Z. Wang, J. Luan, A. Seth, L. Liu, M. You, P. Gupta, P. Rathi, Y. Wang, S. Cao, Q. Jiang, X. Zhang, R. Gupta, Q. Zhou, J. J. Morrissey, E. L. Scheller, J. S. Rudra and S. Singamaneni, *Nat. Biomed. Eng.*, 2021, **5**, 64–76.

71   Z. Bao, S. Lu, D. Zhang, G. Wang, X. Cui and G. Liu, *Adv. Healthcare Mater.*, 2024, **13**, 2303511.

72   P. Zhang, X. Wu, H. Xue, Y. Wang, X. Luo and L. Wang, *Anal. Chim. Acta*, 2022, **1212**, 339911.

73   X. Li, J. Lv, J. Zhao, G. Ling and P. Zhang, *Anal. Chim. Acta*, 2024, **1288**, 342152.

74   J. Ju, C.-M. Hsieh, Y. Tian, J. Kang, R. Chia, H. Chang, Y. Bai, C. Xu, X. Wang and Q. Liu, *ACS Sens.*, 2020, **5**, 1777–1785.

75   R. Mei, Y. Wang, X. Zhao, S. Shi, X. Wang, N. Zhou, D. Shen, Q. Kang and L. Chen, *ACS Sens.*, 2023, **8**, 372–380.

76   Y. Liu, Q. Yu, X. Luo, L. Yang and Y. Cui, *Microsyst. Nanoeng.*, 2021, **7**, 75.

77   P. Bollella, S. Sharma, A. E. G. Cass and R. Antiochia, *Biosens. Bioelectron.*, 2019, **123**, 152–159.

78   C. Moonla, M. Reynoso, A. Casanova, A.-Y. Chang, O. Djassemi, A. Balaje, A. Abbas, Z. Li, K. Mahato and J. Wang, *ACS Sens.*, 2024, **9**, 1004–1013.

79   X. Huang, S. Zheng, B. Liang, M. He, F. Wu, J. Yang, H.-j. Chen and X. Xie, *Microsyst. Nanoeng.*, 2023, **9**, 25.

80   H. Li, G. Wu, Z. Weng, H. Sun, R. Nistala and Y. Zhang, *ACS Sens.*, 2021, **6**, 2181–2190.

81   H. Yoo, H. Jo and S. S. Oh, *Mater. Adv.*, 2020, **1**, 2663–2687.

82   S. Lin, X. Cheng, J. Zhu, B. Wang, D. Jelinek, Y. Zhao, T.-Y. Wu, A. Horrillo, J. Tan, J. Yeung, W. Yan, S. Forman, H. A. Coller, C. Milla and S. Emaminejad, *Sci. Adv.*, 2022, **8**, eabq4539.

83   Y. Wu, F. Tehrani, H. Teymourian, J. Mack, A. Shaver, M. Reynoso, J. Kavner, N. Huang, A. Furmidge, Y. Nie, L. M. Laffel, F. J. Doyle, III, M.-E. Patti, E. Dassau, J. Wang and N. Arroyo-Currás, *Anal. Chem.*, 2022, **94**, 8335–8345.

84   M. Reynoso, A.-Y. Chang, Y. Wu, R. Murray, S. Suresh, Y. Dugas, J. Wang and N. Arroyo-Currás, *Biosens. Bioelectron.*, 2024, **244**, 115802.

85   A. M. Downs, A. Bolotsky, B. M. Weaver, H. Bennett, N. Wolff, R. Polsky and P. R. Miller, *Biosens. Bioelectron.*, 2023, **236**, 115408.

86   X. Li, L. Hu, F. Xu, W. Yu, Y. Wu, J. Deng, Z. Wei, G. Shi and M. Zhang, *Talanta*, 2025, **295**, 128312.

87   K. Zhao, X. Ma, M. Wang, Z. Qu, H. Chen, B. He, H. Chen and B. Zhang, *Anal. Methods*, 2024, **16**, 5665–5675.

88   K. M. Cheung, K.-A. Yang, N. Nakatsuka, C. Zhao, M. Ye, M. E. Jung, H. Yang, P. S. Weiss, M. N. Stojanović and A. M. Andrews, *ACS Sens.*, 2019, **4**, 3308–3317.

89   L. Yue Jing, Y. Fan, B. Zhi Chen, D. Li, Y. Ting He, G. Liang Zhang, L. Liang, J. Du, Y. Wang and X. Dong Guo, *Chem. Eng. J.*, 2024, **502**, 157488.

90   D. D. Zhu, L. W. Zheng, P. K. Duong, R. H. Cheah, X. Y. Liu, J. R. Wong, W. J. Wang, S. T. Tien Guan, X. T. Zheng and P. Chen, *Biosens. Bioelectron.*, 2022, **212**, 114412.

91   M. Razzaghi, J. A. Ninan, M. Azimzadeh, E. Askari, A. H. Najafabadi, A. Khademhosseini and M. Akbari, *Adv. Healthcare Mater.*, 2024, **13**, 2400881.

92   X. Jiang and P. B. Lillehoj, *Microsyst. Nanoeng.*, 2020, **6**, 96.

93   L. Bao, J. Park, B. Qin and B. Kim, *Sci. Rep.*, 2022, **12**, 10693.

94   A. Sena-Torralba, M. Parrilla, A. Hernanz-Grimalt, A. Steijlen, E. Ortiz-Zapater, C. Cabaleiro-Otero, N. López-Riquelme, S. Cerveró-Ferragut, Á. Maquieira, K. De Wael and S. Morais, *Anal. Chem.*, 2024, **96**, 20684–20692.

95   S. Chen, Z. Guo, B. Lu, M. Sun, S. Wang, S. Li, Y. Jiang, Q. Wei, D. Wang and X. Jiang, *Sci. Adv.*, 2025, **11**, eadw2182.

96   J. Xiao, S. Zhang, Q. Liu, T. Xu and X. Zhang, *Sens. Actuators, B*, 2024, **398**, 134685.

97   Y. Cheng, X. Gong, J. Yang, G. Zheng, Y. Zheng, Y. Li, Y. Xu, G. Nie, X. Xie, M. Chen, C. Yi and L. Jiang, *Biosens. Bioelectron.*, 2022, **203**, 114026.

98   T. Abbasiasl, F. Mirlou, H. Mirzajani, M. J. Bathaei, E. Istif, N. Shomalizadeh, R. E. Cebecioglu, E. E. Ozkahraman, U. C. Yener and L. Beker, *Adv. Mater.*, 2024, **36**, e2304704.

99 R. He, H. Liu, T. Fang, Y. Niu, H. Zhang, F. Han, B. Gao, F. Li and F. Xu, *Adv. Sci.*, 2021, **8**, e2103030.

100 M. Sang, M. Cho, S. Lim, I. S. Min, Y. Han, C. Lee, J. Shin, K. Yoon, W.-H. Yeo, T. Lee, S. M. Won, Y. Jung, Y. J. Heo and K. J. Yu, *Sci. Adv.*, 2023, **9**, eadh1765.

101 Q. Wang, Á. Molinero-Fernandez, Q. Wei, X. Xuan, Å. Konradsson-Geuken, M. Cuartero and G. A. Crespo, *ACS Sens.*, 2024, **9**, 3115–3125.

102 M. Parrilla, N. Claes, C. Toyos-Rodríguez, C. E. M. K. Dricot, A. Steijlen, S. Lebeer, S. Bals and K. De Wael, *Biosens. Bioelectron.*, 2025, **289**, 117934.

103 Y. Zhang, G. Zhao, M. Zheng, T. Hu, C. Yang and C. Xu, *Nanoscale*, 2023, **15**, 16493–16500.

104 F. Tehrani, H. Teymourian, B. Wuerstle, J. Kavner, R. Patel, A. Furmidge, R. Aghavali, H. Hosseini-Toudeshki, C. Brown, F. Zhang, K. Mahato, Z. Li, A. Barfidokht, L. Yin, P. Warren, N. Huang, Z. Patel, P. P. Mercier and J. Wang, *Nat. Biomed. Eng.*, 2022, **6**, 1214–1224.

105 X. Li, S. Zheng, M. He, X. Huang, C. Yang, J. Mo, J. Yang, C. Yang, H. Chen and X. Xie, *Innovation*, 2025, **6**, 100781.

106 J. Yang, X. Gong, Y. Zheng, H. Duan, S. Chen, T. Wu, C. Yi, L. Jiang and H. Haick, *Nat. Commun.*, 2025, **16**, 6260.

107 A. Y. Chang, M. Lin, L. Yin, M. Reynoso, S. Ding, R. Liu, Y. Dugas, A. Casanova, G. Park, Z. Li, H. Luan, N. Askarinam, F. Zhang, S. Xu and J. Wang, *Nat. Biomed. Eng.*, 2026, **10**, 94–109.

108 C.-W. Dong, C.-J. Lee, D.-H. Lee, S.-H. Moon and W.-T. Park, *Sens. Actuators, A*, 2024, **367**, 115040.

109 K. J. Krieger, J. Liegey, E. M. Cahill, N. Bertollo, M. M. Lowery and E. D. O'Cearbhaill, *Adv. Mater. Technol.*, 2020, **5**, 2000518.

110 X. Wang, W. Qiu, C. Lu, Z. Jiang, C. Hou, Y. Li, Y. Wang, H. Du, J. Zhou and X. Y. Liu, *Adv. Funct. Mater.*, 2024, **34**, 2311535.

111 G. Stavrinidis, K. Michelakis, V. Kontomitrou, G. Giannakakis, M. Sevrisarianos, G. Sevrisarianos, N. Chaniotakis, Y. Alifragis and G. Konstantinidis, *Microelectron. Eng.*, 2016, **159**, 114–120.

112 H. Ji, M. Wang, Y. Wang, Z. Wang, Y. Ma, L. Liu, H. Zhou, Z. Xu, X. Wang, Y. Chen and X. Feng, *npj Flexible Electron.*, 2023, **7**, 46.

113 J. Li, Y. Ma, D. Huang, Z. Wang, Z. Zhang, Y. Ren, M. Hong, Y. Chen, T. Li, X. Shi, L. Cao, J. Zhang, B. Jiao, J. Liu, H. Sun and Z. Li, *Nano-Micro Lett.*, 2022, **14**, 132.

114 O. P. Singh, A. Bocchino, T. Guillerm, Y. Hu, F. Stam and C. O'Mahony, *Adv. Mater. Technol.*, 2023, **9**, 2301606.

115 C. Zhou, G. Yao, X. Gan, K. Chai, P. Li, J. Peng, T. Pan, M. Gao, Z. Huang, B. Jiang, Z. Yan, K. Zhao, D. Yao, K. Chen and Y. Lin, *npj Flexible Electron.*, 2025, **9**, 77.

116 A. Keirouz, Y. L. Mustafa, J. G. Turner, E. Lay, U. Jungwirth, F. Marken and H. S. Leese, *Small*, 2023, **19**, e2206301.

117 Y. Chen, Z. Fan, N. Shi, B. Cheng, C. Huang, X. Liu, X. Gao and R. Liu, *ACS Appl. Mater. Interfaces*, 2025, **17**, 33451–33464.

118 Y.-C. Yang, Y.-T. Lin, J. Yu, H.-T. Chang, T.-Y. Lu, T.-Y. Huang, A. Preet, Y.-J. Hsu, L. Wang and T.-E. Lin, *ACS Appl. Nano Mater.*, 2021, **4**, 7917–7924.

119 Q. Zhao, E. Gribkova, Y. Shen, J. Cui, N. Naughton, L. Liu, J. Seo, B. Tong, M. Gazzola, R. Gillette and H. Zhao, *Sci. Adv.*, 2024, **10**, eadn7202.

120 Z. Xiang, J. Liu and C. Lee, *Microsyst. Nanoeng.*, 2016, **2**, 16012.

121 Y. Hou, Z. Li, Z. Wang and H. Yu, *Microsyst. Nanoeng.*, 2021, **7**, 53.

122 W. Zhou, Z. Wang, Q. Xu, X. Liu, J. Li, H. Yu, H. Qiao, L. Yang, L. Chen, Y. Zhang, Z. Huang, Y. Pang, Z. Zhang, J. Zhang, X. Guan, S. Ma, Y. Ren, X. Shi, L. Yuan, D. Li, D. Huang, Z. Li and W. Jia, *npj Digit. Med.*, 2024, **7**, 13.

123 Z. Liu, X. Xu, S. Huang, X. Huang, Z. Liu, C. Yao, M. He, J. Chen, H. J. Chen, J. Liu and X. Xie, *Microsyst. Nanoeng.*, 2024, **10**, 72.

124 L. Xing, L. Liu, R. Jin, H. Zhang, Y. Shen, S. Zhang, Z. He, D. Li, H. Ren, Q. Huang, X. Cao, S. Zhang, S. Dong, W. Cheng and B. Zhu, *ACS Appl. Mater. Interfaces*, 2024, **16**, 57695–57704.

125 H. Kim, J. Lee, U. Heo, D. K. Jayashankar, K.-C. Agno, Y. Kim, C. Y. Kim, Y. Oh, S.-H. Byun, B. Choi, H. Jeong, W.-H. Yeo, Z. Li, S. Park, J. Xiao, J. Kim and J.-W. Jeong, *Sci. Adv.*, 2024, **10**, eadk5260.

126 H. Lee, S. Lee, J. Kim, H. Jung, K. J. Yoon, S. Gandla, H. Park and S. Kim, *npj Flexible Electron.*, 2023, **7**, 20.

127 M. Mahmood, S. Kwon, H. Kim, Y. S. Kim, P. Siriaraya, J. Choi, B. Otkhmezuri, K. Kang, K. J. Yu, Y. C. Jang, C. S. Ang and W. H. Yeo, *Adv. Sci.*, 2021, **8**, e2101129.

128 X. Li, S. Wan, T. S. Pronay, X. Yang, B. Gao and C. T. Lim, *Nanoscale Horiz.*, 2025, **10**, 1815–1837.

129 G. Kang, M. Kim, H. Yang, J. Shin, J. Sim, H. Ahn, M. Jang, Y. Kim, H. S. Min and H. Jung, *Adv. Funct. Mater.*, 2023, **33**, 2210805.

130 P. Rivera, F. Della Pelle, J. Stonyte, W. d. C. Martins Antunes de Melo, A. Abouhagger and R. Pauliukaite, *ACS Sens.*, 2025, **10**, 9183–9202.

131 K. Mahato, T. Saha, S. Ding, S. S. Sandhu, A.-Y. Chang and J. Wang, *Nat. Electron.*, 2024, **7**, 735–750.

132 F. Liu, A. Christou, A. S. Dahiya and R. Dahiya, *Adv. Mater.*, 2025, **37**, 2411151.

133 K. Kuruvinashetti, A. Komeili and A. Sanati Nezhad, *Lab Chip*, 2025, **25**, 3879–3920.

134 J. Lee, J. Jeong, V. P. Nguyen, S. Hong, Y. M. Paulus and C. H. Lee, *NPG Asia Mater.*, 2025, **17**, 33.

135 M. M. Paci, T. Saha, O. Djassemi, S. Wu, C. Y. X. Chua, J. Wang and A. Grattoni, *Nat. Rev. Bioeng.*, 2025, **3**, 816–834.

136 X. Li, X. Huang, J. Mo, H. Wang, Q. Huang, C. Yang, T. Zhang, H.-J. Chen, T. Hang, F. Liu, L. Jiang, Q. Wu, H. Li, N. Hu and X. Xie, *Adv. Sci.*, 2021, **8**, 2100827.

137 M. Parrilla, U. Detamornrat, J. Domínguez-Robles, S. Tunca, R. F. Donnelly and K. De Wael, *ACS Sens.*, 2023, **8**, 4161–4170.